We are IntechOpen, the world's leading publisher of Open Access books Built by scientists, for scientists

4,800
Open access books available

122,000
International authors and editors

135M
Downloads

Our authors are among the

154
Countries delivered to

TOP 1%
most cited scientists

12.2%
Contributors from top 500 universities

CLARIVATE ANALYTICS BOOK CITATION INDEX INDEXED

WEB OF SCIENCE™

Selection of our books indexed in the Book Citation Index in Web of Science™ Core Collection (BKCI)

Interested in publishing with us?
Contact book.department@intechopen.com

Numbers displayed above are based on latest data collected.
For more information visit www.intechopen.com

18

Diffraction Gratings for the Selection of Ultrashort Pulses in the Extreme-Ultraviolet

Luca Poletto, Paolo Villoresi and Fabio Frassetto
CNR-National Institute for the Physics of Matter & Dep. of Information Engineering
LUXOR - Laboratory for UV and X-Ray Optical Research
Padova
Italy

1. Introduction

We discuss the use of diffraction gratings to perform the spectral selection of ultrashort pulses in the extreme-ultraviolet and soft X-ray spectral regions, ranging in the 3-100 nm wavelength range. The main application of such a technique is the spectral selection of high-order laser harmonics and free-electron-laser pulses in the femtosecond time scale. We present the design and realization of both single- and double-grating monochromators using an innovative grating geometry, namely the off-plane mount. The performances of existing instruments are shown. The use of diffraction gratings to change the phase properties of the pulse, e.g. to compress it to shorter temporal duration close to the Fourier limit, is also discussed.

Extreme-ultraviolet (XUV) and X-ray photons have been used for many fundamental discoveries and outstanding applications in natural sciences (Wiedermann, 2005). They have played a crucial role in basic research and medical diagnostics, as well as in industrial research and development. The main reason for this success is that the wavelength, which determines the smallest distance one can study with such a probe, is comparable to the molecular and atomic dimension. On the other side, the advent of femtosecond (1 fs = 10^{-15} s) lasers has revolutionized many areas of science from solid-state physics to biology (Diels & Rudolph, 2006). The significance of the femtosecond time regime is that atomic motion which governs structural dynamics, such as phase transitions and chemical reactions, occurs on the vibrational timescale of ~100 fs. While femtosecond optical lasers have offered unique insights into ultra-fast dynamics, they are limited by the fact that the structural arrangement and motion of nuclei are not directly accessible from measured optical properties.

The availability of coherent and tunable sources in the XUV and X-rays with characteristics similar to those of ultrashort lasers in the visible and near-infrared opens the way to a completely new class of experiments both in fundamental and applied research (Patel, 2002). It requires joining the competences in the ultrafast techniques with those on instrumentation and experiments in the XUV and X-rays. The handling of the photons emitted by such sources requires particular attention to the management of high intensity pulses, to the preservation of the ultrashort pulse duration and to the effects of the optical components on the phase of the pulse.

Source: Advances in Solid-State Lasers: Development and Applications, Book edited by: Mikhail Grishin,
ISBN 978-953-7619-80-0, pp. 630, February 2010, INTECH, Croatia, downloaded from SCIYO.COM

Here, we deal with the problem of making the spectral selection of a XUV and soft X-ray pulse while preserving its duration in the femtosecond, or even shorter, time scale. The technique is useful for high-order laser harmonics and free-electron-laser pulses.

High-order harmonics (HHs) generated by the interaction between an ultra-short laser pulse and a gas jet are currently considered as a relevant source of coherent XUV and soft X-ray radiation of very short time duration and high peak brilliance, with important applications in several areas both in fundamental research and in advanced technology (Jaegle, 2006). Owing to the strong peak power of a femtosecond laser pulse, a nonlinear interaction with the gas jet takes place and produces odd laser harmonics (i.e. of order $2n$ +1 with n integer), well above the order of 100. When the laser beam and its second harmonic are used together, a full spectrum of even ($2n$) and odd ($2n$+ 1) harmonics is obtained. In this way a conversion from near-infrared or visible light into XUV and soft-x-ray radiation takes place, giving rise to a XUV source with the same properties of the generating laser in terms of coherence and short pulse duration. The HH spectrum is described as a sequence of peaks corresponding to the harmonics of the fundamental laser wavelength and having an intensity distribution characterized by a vast plateau, whose extension is related to the laser pulse intensity. The radiation generated with the scheme of the HHs generated by laser pulses of a few optical cycles recently become the tool for the investigation of matter with sub-femtosecond, or attosecond, resolution (1 as = 10^{-18} s) (Kienberger & Krausz, 2004; Corkum & Krausz, 2007). The access to this unexplored time domain opens new frontiers in atomic, molecular and solid-state science (Marciak-Kozlowska, 2009), as it becomes possible to do experiments with an unprecedented time resolution and intensity.

Another way to obtain very intense ultrashort and tunable pulses in the XUV is the use of free-electron-laser (FEL) generation. FELs share the same optical properties as conventional lasers but they use different operating principles to form the beam, i.e. a relativistic electron beam as the lasing medium which moves freely through a magnetic structure that induces radiation, the so-called undulator (Saldin et al., 2000). The lack of suitable mirrors in the XUV and X-rays regimes prevents the operation of a FEL oscillator; consequently, FEL emission in the XUV and X-ray has to be obtained in a single pass through the undulator. In this case it is possible to feed an electron beam into the undulators with a much smaller emittance than achievable in storage rings. Some XUV and X-ray FEL facilities are now running worldwide: we can cite FLASH (see http://hasylab.desy.de/facilities/flash/index_eng.html) in Hamburg (Germany) and SLAC (see http://lcls.slac.stanford.edu) in Stanford (USA).

Let us consider an ultrashort pulse of XUV radiation that has a wavelength in the 4-100 nm range and that is mixed with the radiation of different spectral ranges. The spectral selection of such a pulse requires the use of a monochromator. As examples of the experimental problems to be addressed by such an instrument in HH generation, we can cite the extraction of a single harmonic (or a group of harmonics) within a broad HH spectrum to obtain an ultrafast pulse at a suitable XUV wavelength, later to be scanned in a given range. Monochromators can be useful also for FEL radiation, both to increase the spectral purity of the fundamental FEL emission and to select the FEL high-order harmonics at shorter wavelengths while rejecting the most intense fundamental. The monochromator called for this purpose is also called to preserve the pulse temporal duration of the XUV pulse as short as in the generation process. This is crucial in order to have both high temporal resolution and high peak power.

The study and design of such compensated monochromator extends the usual domain of the geometrical optics and XUV diffraction grating mountings to include the analysis of the XUV pulse transformation in both spectrum and spectral phase. The monochromator can be modelled as a filter with a complex frequency response $K(\omega)$, that includes both the spectral transmission and the distorsion in the spectral phase as a function of the frequency (Akhmanov et al. 1992). Since the XUV pulse at the generation may be produced to be close to its transform limit, any modification of its complex spectrum results in a severe time broadening as described by its Fourier transform. For a Gaussian profile with no modulation of either phase or frequency, the product of the spectral width at half-height $\Delta\omega_{1/2}$ times the duration at half-height $\Delta\tau_{1/2}$ has a lower limit expressed by the relation

$$\Delta\omega_{1/2}\Delta\tau_{1/2} = 4\ln 2 = 2.77\,. \tag{1}$$

Two are the conditions that have to be verified by the monochromator to maintain the time duration expressed by Eq. 1 after the monochromatization: 1) the band-pass $\Delta\omega_m$ transmitted by the monochromator has to be greater than the bandwidth of the pulse $\Delta\omega_{1/2}$ and 2) the complex transfer function $K(\omega)$ has to be almost constant within the bandwidth. In case of HH selection, since harmonic peaks are well separated, the first condition is verified if the monochromator selects the whole spectral band of a single harmonic (or a group of them), so no modifications in the Fourier spectrum are induced. The case of FEL radiation is also similar: the bandwidth of the monochromator has to be larger than the intrinsic FEL bandwidth. The second condition is almost always verified if the monochromator is realized by reflecting optics: the variations of reflectivity of the coating within the bandwidth of the pulse are usually negligible, so $K(\omega)$ can be considered almost constant, although lower than unity.

2. Grating monochromators for spectral selection of ultrashort pulses

The simplest way to obtain the spectral selection of ultrashort pulses with very modest time broadening is the use of a multilayer mirror in normal incidence, which does not alter the pulse time duration up to fractions of femtosecond and is moreover very efficient: in fact, the functions of selecting a single spectral pulse and focusing it can be demanded to a single concave optics, maximizing then the flux. The choice of the type of multilayer can be made among many couple of materials (i.e. the spacer and the absorber) to optimize the response in a given spectral region (e.g. see http://www-cxro.lbl.gov/multilayer/survey.html). Monochromators with one (Wieland et al. 2001) or two (Poletto & Tondello, 2001) multilayer mirrors have been proposed and realized. The main drawback of the use of multilayer optics is the necessity of many different mirrors to have the tunability on a broad spectral region.

The spectral selection of XUV ultrashort pulses can also be accomplished by an ordinary diffraction grating used in reflection mode. In this case, the major mechanism that alters the time duration of the pulse is the difference in the lengths of the optical paths of the rays diffracted by different grating grooves. In fact, a single grating gives inevitably a time broadening of the ultrafast pulse because of the diffraction: the total difference in the optical paths of the rays diffracted by N grooves illuminated by radiation at wavelength λ is $\Delta OP = Nm\lambda$, where m is the diffracted order. The effect is schematically illustrated in Fig. 1. It follows that the longer the exposed area of the grating and the higher the groove density,

the longer is the time difference between the arrival of the ray diffracted from the first illuminated groove and that diffracted from the last one. As an order-of-magnitude estimate, let us consider a 300 gr/mm grating illuminated by radiation at 40 nm over a length of 10 mm at half intensity; the total number of grooves involved in the diffraction is 3000, corresponding to a maximum delay in the first diffracted order of 120 mm, i.e. 400 fs full-width-at-half-maximum (FWHM). This delay is usually irrelevant for picosecond pulses, but, in case of femtosecond pulses, it reduces dramatically both the time resolution capability and the peak intensity at the output. Nevertheless, single-grating monochromators can be adopted for the spectral selection of ultrashort pulses because of the simplicity of the design and the high efficiency due to the use of a single optical element. In fact, in the XUV and soft X-ray spectral region the reflectivity is usually poor and conventional schemes generally use a single grating. Furthermore, a time resolution in the 100-300 fs time scale can be tolerated on many pump-probe experiments, that is in the range of the temporal response of low-density gratings.

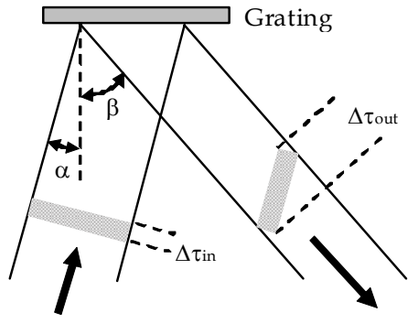

Fig. 1. Schematic illustration of the tilt of the intensity wavefront of an ultrashort pulse diffracted by a grating in the classical diffraction geometry. The incidence angle is indicated as α, the diffracted angle as β, the pulse width at the input as $\Delta\tau_{in}$, the pulse width at the output as $\Delta\tau_{out}$. The broadening is $\Delta OP = Nm\lambda = N\sigma^{-1}(\sin\alpha - \sin\beta)$, where σ is the grating groove density.

The temporal broadening given by a grating poses a problem that cannot be solved with conventional monochromator designs. To select effectively a portion of an extended spectrum without introducing a difference in the optical path length between different rays in the beam, one must use a so called time-delay compensated optical mounting, which involves the use of two gratings in a subtractive configuration to compensate for the dispersion. In the following, such a configuration will be defined as *Time-Delay Compensated (TDC) monochromator*, in the sense that the second grating compensates for the time and spectral spread introduced by the first one. These concepts are well known in the fields of chirped pulse laser amplification and, more generally, propagation of ultrafast light pulses (Walmsley, 2001) and are here discussed in the XUV spectral domain.

From the point of view of the ray paths, two are the conditions that the design must comply: 1) the differences in the path lengths of rays with the same wavelength but with different entrance directions within the beam aperture that are caused by the first grating must be compensated by the second grating, and 2) two rays at different wavelengths within the spectrum of the pulse to be selected have to be focused on the same point, i.e. the global spectral dispersion has to be zero. Both these conditions are satisfied by a scheme with two

equal concave gratings mounted with opposite diffraction orders (Villoresi, 1999): the incidence angle on the second grating is equal to the diffraction angle of the first grating. The spectral selection is performed by a slit placed in an intermediate position between the gratings, where the radiation is focused by the first grating. In the design, only two optical elements are used, namely the concave gratings, since the grating itself provides both the spectral dispersion through diffraction and the focusing due to the curvature of the surface. The schematic of the TDC configuration in case of using two toroidal gratings at normal incidence in the classical geometry is shown in Fig. 2.

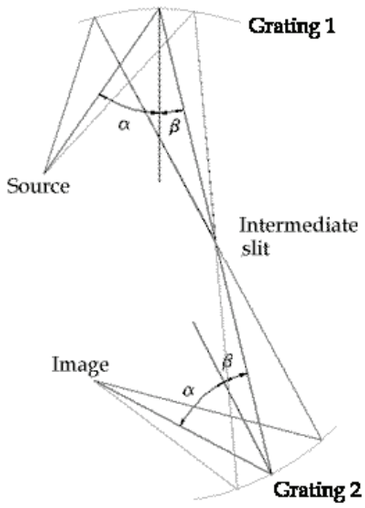

Fig. 2. Schematic of the TDC configuration with two toroidal gratings used at normal incidence.

This design has been proved to be very effective in time compensation of few femtoseconds or even lower for wavelengths longer than ≈40 nm, where the normal-incidence reflectivity of conventional coatings is high so that normal-incidence configurations can be adopted. It can be shown by ray-tracing simulations that a TDC monochromator in the Seya-Namioka mounting can be operated in the 40-100 nm region with residual broadening at the output in the 0.5-1 μm range, i.e. 1-3 fs (Villoresi, 1999). The main advantages of this design are the simplicity, due to the use of only two optical elements, the tunability in a broad spectral band by a simple rotation of both gratings and the possibility of being operated also in spectral regions where multilayer-coated optics are not available (e.g. for wavelengths higher than 60 nm). Unfortunately, the main drawback of using two normal-incidence gratings is the low efficiency in the XUV. By choosing a suitable XUV coating (e.g. gold or platinum), the efficiency of a single grating can be estimated in the 0.1-0.2 range, so the monochromator efficiency results 0.01-0.04.

For wavelengths below ≈35 nm, the normal-incidence configuration cannot be adopted because of the low reflectivity of conventional coatings in normal incidence. Therefore, the gratings have to be operated in grazing incidence. The compensation in this case is harder, due to the intrinsic difficulties arising from grazing-incidence mountings, which are very sensitive to aberrations and misalignments. A configuration with two toroidal gratings has already been presented and discussed (Villoresi, 1999). The time compensation is again very effective, but once the grating radii and the subtended angle are chosen, the compensation is

optimum only in a very narrow spectral region, so the tunability is impaired unless changing the geometry for different spectral regions. Also in this case, the global efficiency of the monochromator is expected to be rather poor. The efficiency is obviously the major factor discriminating among different monochromators: an instrument with low output flux could be not useful for scientific experiments.
We can summarize the main differences between single- and double-grating monochromators as follows: 1) the single-grating design is simpler and more efficient, but its temporal response is longer; 2) the double-grating design is more complex and less efficient, but the temporal response can be as short as fractions of femtosecond. The choice between the two configurations has to be done as a trade-off between photon flux and time resolution.

3. The off-plane grating geometry: characteristics and performance

The main limitation to the use of TDC configurations with gratings in the classical mount is the poor efficiency of the design and the difficulty in achieve a broad tunability in grazing incidence. Both these drawback are overtaken by adopting a different geometry, the so called off-plane mount for gratings at grazing incidence. This mount differs from the classical one in that the incident and diffracted wave vectors are almost parallel to the grooves (Cash, 1982). The geometry is shown in Fig. 3.

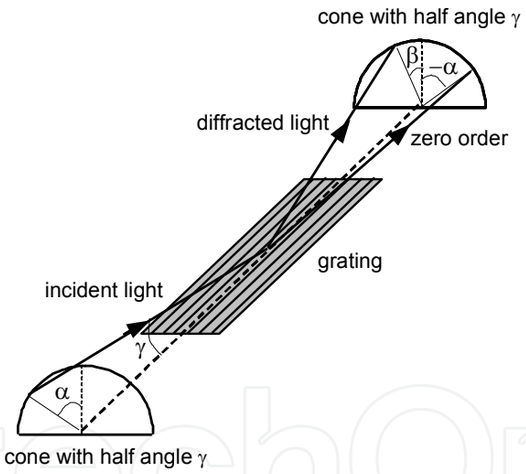

Fig. 3. The off-plane geometry.

The direction of the incoming rays is described by two parameters, the altitude and the azimuth. The altitude γ is the angle between the direction of the incoming rays and the direction of the grooves. It defines the half-angle of the cone into which the light is diffracted: all the rays leave the grating at the same altitude angle at which they approach. The azimuth α of the incoming rays is defined to be zero if they lie in the plane perpendicular to the grating surface and parallel to the rulings, so $-\alpha$ is the azimuth of the zero order light. Let β define the azimuth of the diffracted light at wavelength λ and order m. The grating equation is written as

$$\sin\gamma\,(\sin\alpha + \sin\beta) = m\lambda\sigma \tag{2}$$

where σ is the groove density.
The blaze condition of maximum efficiency is described as in the classical diffraction geometry: the light has to leave the grating in such a way that it performs a specular reflection on the groove surface, that is $\alpha + \beta = 2\delta$, where δ is the grating blaze angle. In addition, shadowing effects from adjacent grooves must be avoided, that is $\alpha = \delta$. It follows that the highest efficiency of a blazed grating in the off-plane mount is achieved when $\alpha = \beta = \delta$, that is when each groove of the grating is seen by the incident ray as a portion of a plane mirror. The grating equation in the blaze condition becomes $2 \sin\gamma \sin\delta = m\lambda\sigma$, indicating that both incident and diffracted rays at the blaze wavelength lie in a plane that is parallel to the direction of the grooves and also perpendicular to their surface.
It has been theoretically shown and experimentally measured that the diffraction efficiency of the off-plane mount is close to the reflectivity of the coating, so much higher efficiencies than in the classical diffraction mount can be obtained in the XUV (Petit, 1980). The off-plane mount is then an appropriate candidate to realize XUV and soft X-ray monochromators for ultrashort pulses with high efficiency (Poletto, 2004a; Pascolini et al., 2006).
Gratings in the off-plane mount are usually operated in parallel light. Therefore, a monochromator requires at least three optical elements: 1) a first concave mirror at grazing incidence that collimates the light coming from the entrance slit, 2) the plane grating and 3) a second concave mirror that focuses the light on the exit slit. In order to keep the grating on-blaze for each wavelength (i.e. maximum efficiency over the whole bandwidth of operation), the grating equation in blaze condition $2 \sin\gamma \sin\delta = m\lambda\sigma$ should be satisfied in the entire spectral bandwidth: this requires the variation of the altitude γ, since the blaze angle δ is fixed. In this case, the wavelength scanning is rather complex: the grating is translated along an axis perpendicular to its surface, so the altitude is changed. In order to keep a constant output direction toward the focusing mirror, two additional plane mirrors are inserted in the design, and are rotated with the wavelength (Werner & Wisser, 1984). A schematic of the monochromator is shown in Fig. 4(a).

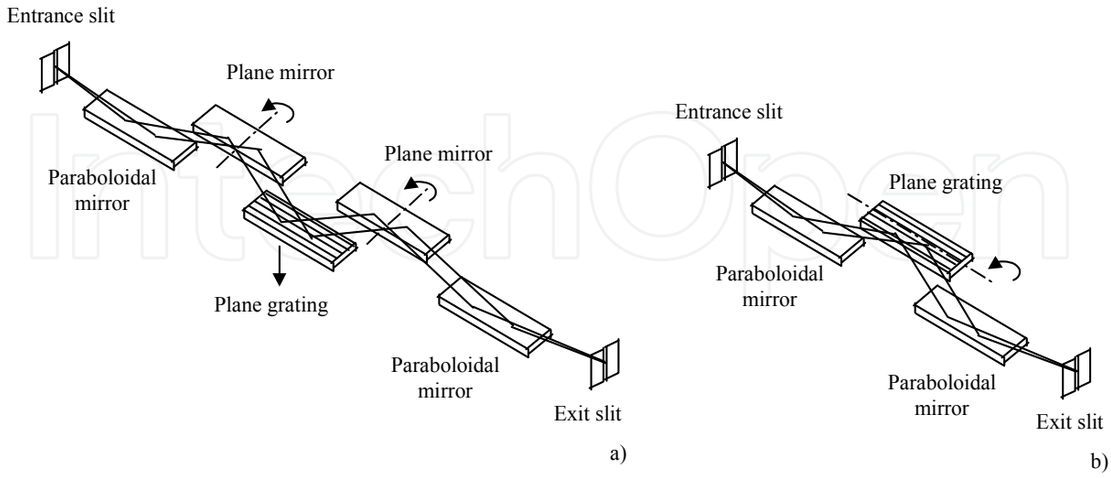

Fig. 4. Monochromator with plane gratings in the off-plane mount. a) Grating on-blaze at each wavelength: the wavelength scanning is performed by changing the altitude and keeping constant the azimuth. b) Grating on-blaze at one wavelength: the wavelength scanning is performed by changing the azimuth and keeping constant the altitude.

A simpler layout consists in performing the wavelength scanning by rotating the grating around an axis passing through the grating center and parallel to the groove direction, so the azimuth is changed while the altitude γ is kept constant (Werner & Wisser, 1984). For each wavelength, the relation $\alpha = \beta$ is satisfied, so the grating equation is expressed as

$$2 \sin\gamma \sin\alpha = m\lambda\sigma. \quad (3)$$

The blaze condition of maximum efficiency is satisfied only at the wavelength λ_B for which $\alpha(\lambda_B) = \beta(\lambda_B) = \delta$: $\lambda_B = 2 \sin\gamma \sin\delta/m\sigma$. At different wavelengths, the efficiency decreases because the grating is operated off-blaze. No additional plane mirrors are required in this configuration. A schematic of the monochromator is shown in Fig. 4(b).

The main advantage the off-plane mount is the high efficiency in the XUV and soft X-ray domains. We summarize here some experimental results obtained on gratings to be used for the spectral selection of ultrashort pulses. The efficiency of three plane gold-coated gratings manufactured by Richardson Gratings (Newport) has been measured in the 10-130 nm spectral region at the beamline BEAR of the ELETTRA Synchrotron (Trieste, Italy). The gratings were operated in the same way as in geometry shown in Fig. 4(b): the altitude angle γ is kept constant and, for each desired wavelength, the azimuth angle α is selected from Eq. 3 to have $\alpha = \beta$. The condition of maximum efficiency is satisfied only at the blaze wavelength. Far from it, the efficiency decreases. The efficiency is here intended as the absolute efficiency, i.e. the ratio between the flux measured in the diffracted order and the total flux on the grating. The parameters of the measurements are resumed in Tab. 1.

Grating	*Grooves/mm*	*Blaze angle* δ	*Altitude angle* γ	*Blaze wavelength (1st order)*	*Wavelength*
#1	600	7°	11.4°	80 nm	50-130 nm
#1	600	7°	3°	21.5 nm	10-45 nm
#2	400	9.7°	3°	45 nm	20-90 nm
#3	400	4.5°	6.6°	45 nm	20-90 nm

Table 1. Gratings under test in the off-plane geometry.

The efficiency curves of grating #1 are shown in Fig. 5. The peak efficiency at the blaze wavelength is about 0.5. The grating is very selective when operated on-blaze: at 1st order blaze wavelength, both 0th and 2nd orders are negligible. As expected, 1st order efficiency decreases when the grating is rotated off-blaze to select other portions of the spectrum. At wavelengths longer than 1st order blaze wavelength $\lambda > \lambda_{B\text{-}1st}$, where the grating blaze angle is lower than the azimuth angle $\delta < \alpha$, the radiation is split between 1st and 0th orders. 2nd order efficiency is null because 2nd order diffraction is far from the blaze condition. At wavelengths shorter than 1st order blaze wavelength $\lambda < \lambda_{B\text{-}1st}$, where the grating blaze angle is higher than the azimuth angle $\delta > \alpha$, the radiation is split between 1st and 2nd orders, for which the blaze condition would be $\delta = (\alpha + \beta_{2nd})/2$. 2nd order efficiency increases and reaches its maximum at $\lambda_{B\text{-}1st}/2$, that is the 2nd order blaze wavelength. Then, the same grating can be operated in a large spectral region with high efficiency using 1st order diffraction around the 1st order blaze wavelength, and 2nd order diffraction around 2nd order blaze wavelength.

The efficiency curves of grating #2 and #3 operated in the 20-90 nm region are shown in Fig. 6. The peak efficiency of grating #2 is exceptionally high, even more than 0.7. Again, the gratings are very selective when operated on-blaze.

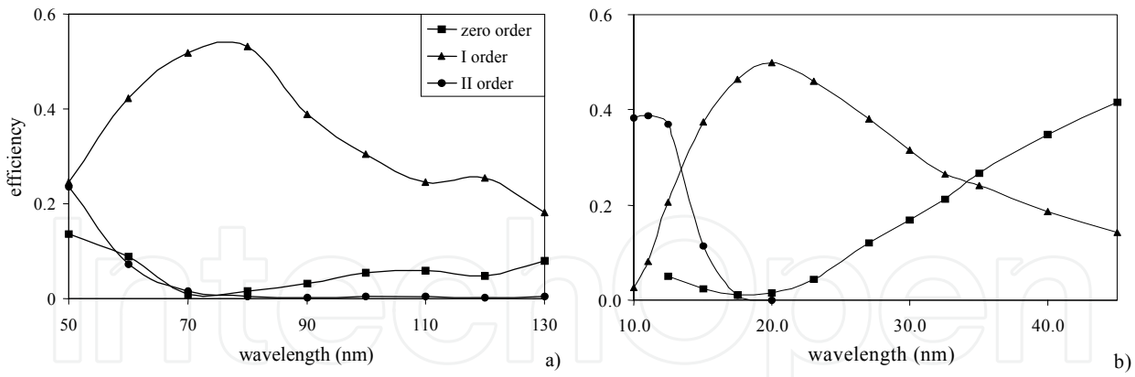

Fig. 5. Efficiency curves of grating #1: a) grating operated at $\gamma = 11.4°$ in the 50-130 nm region; b) grating operated at $\gamma = 3°$ in the 10-45 nm region.

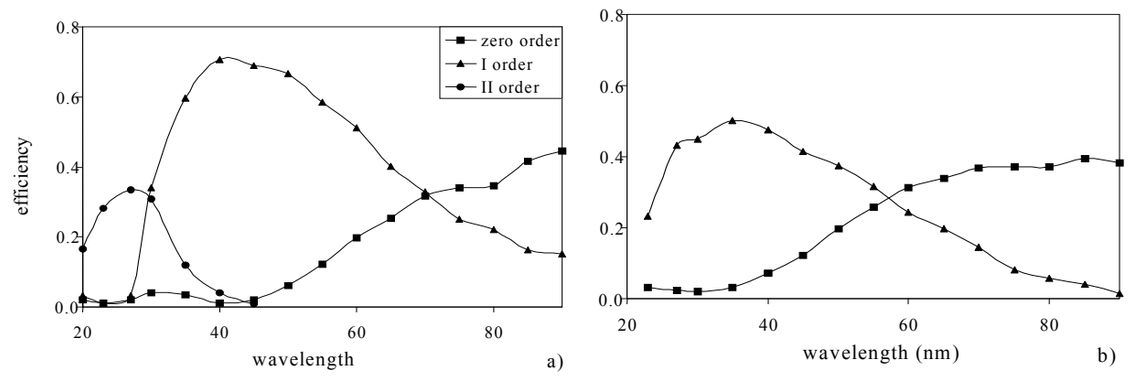

Fig. 6. Efficiency curves of grating #2 and #3 operated at $\gamma = 3°$ in the 20-90 nm region: a) grating #2; b) grating #3.

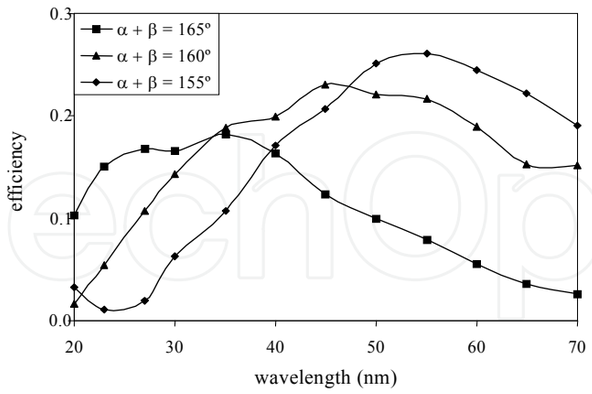

Fig. 7. Efficiency curves of grating #3 operated in classical configuration at constant inclusion angle, i.e. $\alpha + \beta = K$.

The diffraction efficiency of grating #3 was also measured in the classical grazing-incidence configuration, when the incoming rays are perpendicular to the grooves. The measurements were performed at constant inclusion angle, i.e. $\alpha + \beta = K$, where α is the incidence angle and β the diffraction angle. The curves in the 20-70 nm region are shown in Fig. 7. The

maximum efficiency depends on the inclusion angle and ranges in the 0.18-0.25 interval. With respect to the off-plane mount, the efficiency of the same grating is lower by a factor two to three. This confirms the advantage of the off-plane mount in terms of high throughput from the monochromator.

4. Design of a single-grating monochromator in the off-plane geometry

The single-grating configuration in the off-plane geometry adopts a plane grating operated in parallel beam and two concave mirrors, as shown in Fig. 4(b). The first mirror collimates the light coming from the point source; the grating is operated in the condition $\alpha = \beta$; the second mirror focuses the diffracted light on the exit slit. All the optical elements are operated in grazing incidence. The wavelength scan is provided by rotating the grating around an axis passing through the grating center and parallel to the direction of the grooves, as shown in Eq. 3. In this design, the azimuth changes with the wavelength while the altitude γ is kept constant, so that the maximum efficiency condition is fulfilled only at the blaze wavelength $\lambda_B = 2 \sin\gamma \sin\delta / m\sigma$ which depends on the blaze angle of the grating profile. At different wavelengths, the efficiency decreases because the grating is operated off-blaze. Such a mount is very efficient in a broad spectral region, as shown from the experimental curves of Fig. 5 and Fig. 6.

The driving parameter is the FWHM bandwidth at the output $\Delta\lambda_{FWHM}$, calculated at first diffraction order as

$$\Delta\lambda_{FWHM} = \frac{W}{\sigma\, q_{out}} \tag{4}$$

where W is the width of the exit slit, that is typically in the range 50-200 μm, and q_{out} is the length of the output arm of the focusing mirror, i.e. the distance between the center of the mirror and the exit slit, that is typically in the range 300-500 mm. The bandwidth has to be as broad as the bandwidth of the ultrashort pulse to be selected, to avoid the broadening of the pulse duration as expressed in Eq. 1.

In case of selection of the single harmonic Hn (n odd) within the HH spectrum, i.e. to have the adjacent harmonics completely filtered out, the slit aperture is

$$W = \sigma\, q_{out}\, \frac{\Delta\lambda_{H(n-2)-H(n+2)}}{2} \cong \sigma\, q_{out}\, \lambda_0\, \frac{2}{n^2} \tag{5}$$

where $\Delta\lambda_{H(n-2)-H(n+2)}$ indicates the difference in wavelength between the two harmonics H(n-2) and H(n+2), that is expressed by $\Delta\lambda_{H(n-2)-H(n+2)} = 4\lambda_0 / n^2$ where λ_0 is the laser fundamental wavelength, that is 800 nm for the Ti:Sa laser.

Once the geometric parameters have been chosen (i.e. output arm and slit width), the spectral resolution $\mathcal{R} = \lambda/\Delta\lambda$ given by the off-plane mount is proportional only to the grating groove density. On the contrary, the resolution given by the classical mount is proportional also to the inverse of the cosine of the diffraction angle, so at extreme grazing conditions the resolution becomes higher for a given groove density. Since the resolution of the off-plane mount is independent from the grazing angle, low-resolution configurations in the off-plane mount can be designed even at extreme grazing incidence for XUV and soft X-rays.

The instrumental temporal response of the off-plane grating $\Delta\tau_{FWHM}$ depends on the groove density and on the illuminated area

$$\Delta\tau_{FWHM} = \frac{\sigma\lambda q_{in}\mathcal{D}_{FWHM}}{c} \tag{6}$$

where $\mathcal{D}_{FWHM}$ is the FWHM divergence of the source, c is the speed of light in vacuum and q_{in} is the length of the input arm of the collimating mirror, i.e. the distance between the source and the center of the mirror. The mirrors have typically a toroidal shape, then the aberrations at the output are minimized if they have equal arms, i.e. $q_{in} = q_{out} = q$.
Since the grooves are almost parallel to the input direction, the number of grooves that are illuminated in the off-plane mount is independent from the altitude angle, $N = \sigma\, q\, \mathcal{D}_{FWHM}$. Therefore, once the groove density has been defined, the temporal broadening is univocally determined. This allows to operate the grating even at extreme grazing conditions without changing its temporal response. On the contrary, the number of grooves illuminated in the classical mount is proportional to the inverse of the cosine of the incident angle, so the temporal response at grazing incidence changes at each wavelength depending on the working conditions. Then, the operation in the off-plane mount gives more flexibility than the classical mount in the choice of the incidence angle at very short wavelengths and a temporal response that varies linearly with the wavelength.

Spectral region	10-80 nm
Concave mirrors	Toroidal surfaces
Grazing angle	3°
Arms	300 mm
Gratings	4 plane gratings
Altitude	3.5°
Grating 1	Low resolution, long wavelengths
Groove density	60 gr/mm
Blaze angle and blaze wavelength	1.3°, 45 nm
Plate factor	55.6 nm/mm
Grating 2	Low resolution, short wavelengths
Groove density	120 gr/mm
Blaze angle and blaze wavelength	1.1°, 20 nm
Plate factor	27.8 nm/mm
Grating 3	Medium resolution, long wavelengths
Groove density	300 gr/mm
Blaze angle and blaze wavelength	6.5°, 46 nm
Plate factor	11.1 nm/mm
Grating 4	Medium resolution, short wavelengths
Groove density	500 gr/mm
Blaze angle and blaze wavelength	4.7°, 20 nm
Plate factor	6.7 nm/mm
Exit slit	50-300 μm

Table 2. Parameters of the monochromator of the ASTRA-ARTEMIS beamline at Rutherford Appleton Laboratory (UK).

It is clear from Eq.s 4-5 that the higher the spectral resolution, the longer the temporal response. The aim of the optical design is to find the best trade-off between spectral resolution and temporal broadening.

As an example, let us report the characteristics of a low-resolution monochromator for the spectral selection of HHs in the 80-10 nm region (Frassetto et al., 2008). The monochromator has been realized in the LUXOR laboratory in Padova (Italy) and is installed in the ASTRA-ARTEMIS beamline of the Central Laser Facility of the Rutherford Appleton Laboratory (UK). The design parameters are resumed in Tab. 2. The monochromator is operated without an entrance slit: the HH generation point is the source point for the instrument. It has four different gratings to cover the 10-80 nm region with different spectral resolutions. The gratings are mounted on a swivel motorized stage for the rotation and a linear motorized stage for the selection of the grating to be used. The radiation exiting from the slit is finally focused to the experimental chamber by a suitable toroidal mirror at grazing incidence. A schematic of the monochromator and a picture of the instrument are shown in Fig. 8.

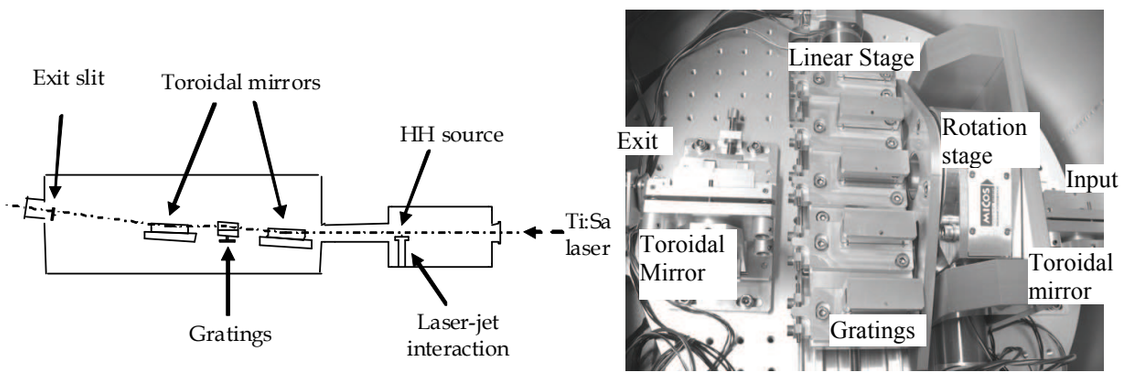

Fig. 8. The monochromator for HHs of the beamline ASTRA-ARTEMIS at Rutherford Appl. Lab. (UK). a) Schematic. b) Internal view of the monochromator chamber.

The pulse duration of the ultrashort pulse is altered by the use of the grating. The FWHM spread of the optical paths at the output of the monochromator is calculated from Eq. 6 as 15-25 fs for the two low-resolution gratings and 45-70 fs for the two medium-resolution gratings. In case of broad bandwidth, as that needed to select the whole single harmonic, time-resolved experiments with resolution of few tens of femtoseconds can be supported by the monochromator in the off-plane mount.

One of the calibration spectra taken at LUXOR with a hollow-cathode XUV lamp and a HH spectrum measured at ASTRA-ARTEMIS are shown in Fig. 9. The spectra have been acquired by a channeltron (CEM) detector mounted after the exit slit through the grating rotation. The spectral resolution is very close to the values predicted by the ray-tracing calculations.

The efficiency of the instrument is here defined as the ratio between the output and the entrance flux: it includes the reflectivity of the two toroidal mirrors and the grating diffraction efficiency. The peak values measured at the blaze wavelength of each grating are in the 0.20-0.28 range. These are extremely good values in the XUV, confirming the benefits of the off-plane mount in terms of expected throughput.

Finally, the output photon flux has been measured by an absolutely calibrated XUV photodiode to be as high as $2.5 \cdot 10^6$ photons/shot on H25 (32 nm) focused on a spot of 150 μm in diameter. Taking 50 fs as a conservative estimate of the duration, we have about $1.4 \cdot 10^6$ W/cm^2 at 32 nm.

With respect to monochromators adopting the classical grating geometry, the off-plane mount gives higher efficiency and shorter temporal response. This innovative configuration can be used for the spectral selection of ultrashort pulses in a single-grating configuration when a monochromatic beam in the time scale of few tens of femtoseconds is required at the output.

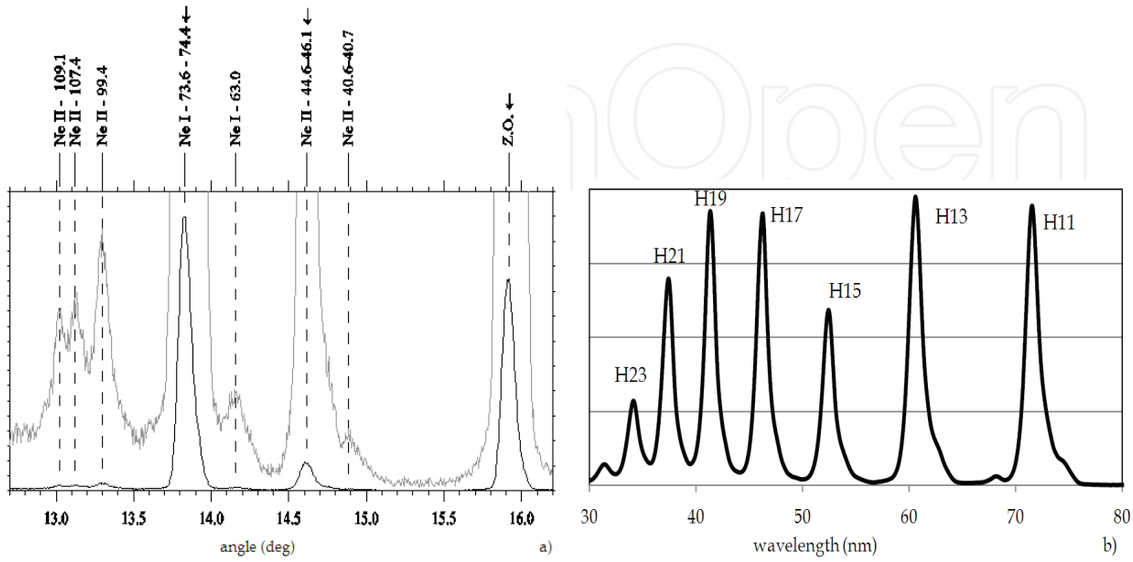

Fig. 9. Spectra taken with the single-grating monochromator in the off-plane mount. a) Spectrum of the emission lines of the hollow-cathode lamp with Ne gas; the over-imposed plots refer to spectral lines with lower intensities. b) HH spectrum generated in Argon with 1-mJ 25-fs Ti:Sa laser operated at 1 kHz repetition rate.

5. Design of a double-grating monochromator in the off-plane geometry

The single-grating monochromator gives temporal resolution in the 20-100 fs range. If the duration of the output pulse has to be preserved as short as in the generation process, a double-grating configuration has to be adopted. Here we will discuss the design and realization of a TDC monochromator using plane gratings in the off-plane mount.

The off-plane geometry can be applied to the design of TDC monochromators using two equal gratings operated at the same altitude and azimuth (Poletto, 2004b; Poletto & Villoresi, 2006). A schematic of the configuration with plane gratings, requiring six optical elements, is shown in Fig. 10. The monochromator is divided in two equal sections, each of them with two toroidal mirrors and a plane grating. The first section gives a spectrally dispersed image of the source on the intermediate plane, where a slit carries out the spectral selection. Only a selected portion of the spectrum is propagating through the slit toward the second section that compensates both for the temporal spread and spectral dispersion and gives a spectrally selected stigmatic image on its focal plane.

The first mirror of each section acts as the collimator, the second mirror as the condenser. The four mirrors are operated at equal grazing angle and unity magnification to minimize the aberrations, i.e. the input arm of each of the two collimators is equal to the output arm of each of the two condensers. With reference to Fig. 10, the term "*input arm*" refers to the two collimators and indicates the distance between the source and the vertex of mirror M1 and

the distance between the slit and the vertex of mirror M3; the term "*output arm*" refers to the two condensers and indicates the distance between the vertex of mirror M2 and the slit and the distance between the vertex of mirror M4 and the output focal point. The four mirrors are then equal, i.e. they have the same tangential and sagittal radii.

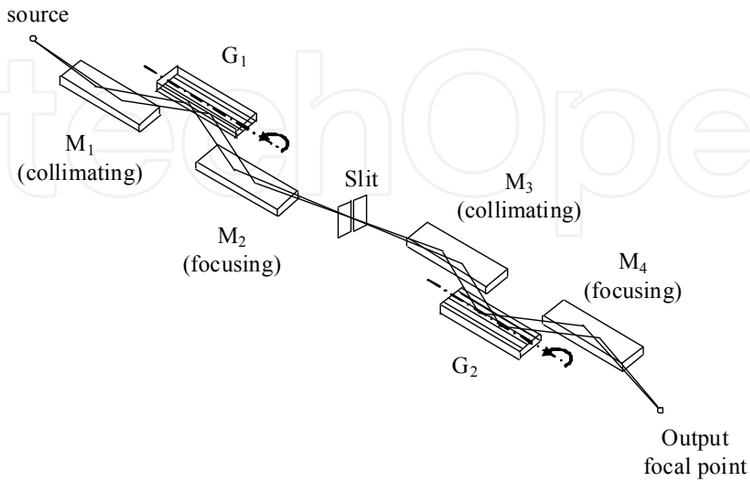

Fig. 10. Schematic of a time-delay compensated monochromator with plane gratings in the off-plane mount.

The wavelength scanning is performed by rotating the gratings around an axis tangent to their vertex and parallel to the grooves, as in the single-grating design already discussed. The axis of rotation is parallel to the plane which defines the direction of propagation of light. The rotation is defined to be zero when the two gratings are operated as mirrors, i.e. $\alpha=\beta=0$, and positive if the grating is rotated clockwise when looking to it from the direction of propagation of the light. The rotation $\Delta\alpha$ to select the wavelength λ is calculated from the grating equation as

$$\Delta\alpha = \pm\arcsin\left(\frac{\lambda\sigma}{2\sin\gamma}\right) \tag{7}$$

where the two gratings have opposite rotations to realize the TDC configuration. The bandwidth transmitted by the intermediate slit is given by Eq. 4 and Eq. 5.

It can be demonstrated (Poletto, 2009) that the off-plane mount is more robust than the classical one in terms of the tolerances in the alignment to achieve time-delay compensation in the femtosecond time scale.

A TDC monochromator for the selection of HHs in the 20-70 nm region has been designed and realized at LUXOR (Padova) and is now installed in the Department of Physics of Politecnico Milano (Italy) (Poletto & Villoresi, 2006; Poletto et al., 2007). Its characteristics are resumed in Tab. 3. The toroidal mirrors are operated with 250 mm arms at 3° grazing angle to have high reflectivity in the whole spectral region of operation. Two 400 gr/mm plane gratings at 3° altitude angle are used. The accepted angular aperture is 10 mrad.

The optical performance and the analysis of the compensation of the optical paths have been carried out by a ray-tracing program suitable to simulate the temporal response of monochromators. The results of the simulations are reported in Tab. 4 for some of the

harmonics. The FWHM spreads of the path lengths in a single harmonic are shown both at the slit plane and at the output plane. The differences in the path lengths are almost completely cancelled by the compensated configuration. The residual spread at a fixed harmonic is less than one femtosecond at the shortest wavelengths of the spectral interval of operation.

Spectral region	15-70 nm
Concave mirrors	Toroidal surfaces
Input/output arms	350 mm
Grazing angle	3°
Gratings	**Plane**
Groove density	400 grooves/mm
Altitude angle	3°
Blaze angle and blaze wavelength	6.5°, 30 nm (1st order)

Table 3. Parameters of the TDC monochromator.

Harmonic order	FWHM ΔOP_{SLIT}	FWHM ΔOP
H15 (53.3 nm)	32 μm (105 fs)	0.6 μm (2.0 fs)
H19 (42.1 nm)	25 μm (85 fs)	0.4 μm (1.2 fs)
H31 (25.8 nm)	15 μm (50 fs)	0.15 μm (0.5 fs)

Table 4. Ray-tracing simulations of the TDC monochromator: ΔOP_{SLIT} and ΔOP are the spreads of the optical paths respectively in the intermediate slit plane and at the output.

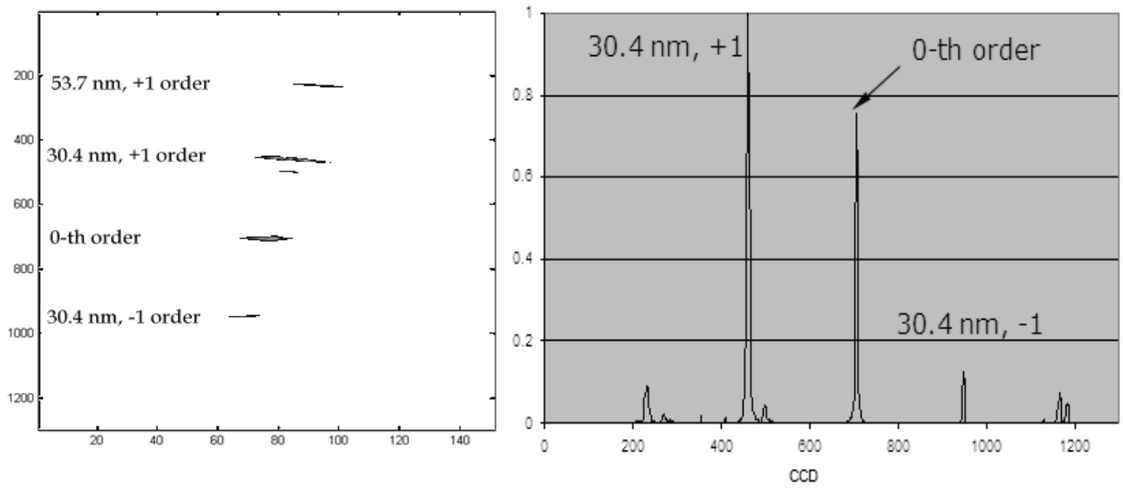

Fig. 11. Spectrum of He emissions from an hollow-cathode lamp, taken by a XUV-enhanced CCD detector placed in the output plane. Both gratings are operated in the condition $\alpha = 0$. A cross section along the CCD column num. 70 is shown on the right.

One of the spectra of He emissions taken during the calibration phase by a CCD camera placed in the output plane is shown in Fig. 11. The spectrum has been acquired by using both gratings in the condition $\alpha = 0$. The first section acts simply as a relay section that focuses the 0th order radiation on the intermediate slit. The grating of the second section disperses the spectrum on an arc, as expected from the off-plane geometry. Furthermore, it

is clear that the most intense spectral line is the HeII 30.4 nm emission, indicating that the blaze wavelength of the gratings is close to 30 nm, according to the optical design.
A HH spectrum is shown in Fig. 12. The spectrum has been acquired by a CEM detector placed at the output. The different wavelengths have been scanned by the rotation of both gratings. HHs from H13 to H25 are clearly distinguished.
The absolute efficiency of the monochromator was measured using the radiation from a hollow-cathode spectral lamp, emitting lines with a narrow spectral profile. The region of operation has been characterized by using Neon and Helium gases. The efficiency has been obtained from the comparison of the input and output power at a given wavelength. The total transmission efficiency in the spectral region of operation is shown in Fig. 13. The peak efficiency at 30 nm is about 0.17, whereas for an extended part of the curve it is above 0.10. This efficiency is exceptionally high for a six-optics setup in grazing incidence and is mostly the result of the off-plane mount of the gratings.

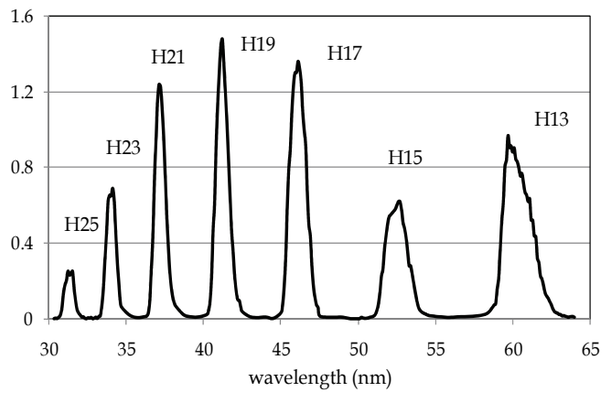

Fig. 12. HH spectrum generated in Argon with 0.3-mJ 25-fs Ti:Sa laser operated at 1 kHz repetition rate.

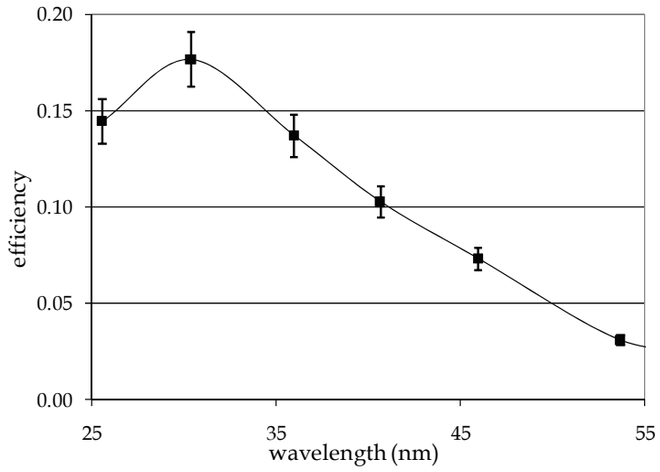

Fig. 13. Absolute efficiency of the TDC monochromator. Both gratings are operated in 1st diffraction order.

The absolute flux at the output has been measured by an absolutely calibrated XUV photodiode. The flux at the output of the monochromator ranges from $5 \cdot 10^5$ photons/shot at

H17 to $1.3 \cdot 10^6$ photons/shot at H23, generated in Argon with 0.3-mJ 25-fs Ti:Sa laser operated at 1 kHz repetition rate.

The XUV spot size at the output has been measured to be around 150 μm FWHM in diameter. Despite the presence of six optical elements, the TDC monochromator gives high-quality imaging properties.

Finally, the temporal profile of the XUV pulses at the output of the monochromator has been measured by a cross-correlation technique (Poletto et al., 2008a). The experimental setup is shown in Fig. 14. The Ti:Sa laser pulse (25-fs duration and 1-kHz repetition rate) is split in two parts using a drilled mirror with a central hole. The inner part is focused into the Argon cell for HH generation. The XUV radiation propagates inside the monochromator that realizes the spectral selection of one of the HHs. Both the XUV beam and the outer annular part of the infrared beam, after a variable-delay stage, are focused onto the same Argon jet that is located in the output focal point of the monochromator for the cross-correlation measurement. The photoelectrons generated by single-photon absorption of the XUV pulses are collected by a time-of-flight spectrometer. The duration of the XUV harmonic pulses is obtained by measuring the cross-correlation between the XUV and the IR pulses.

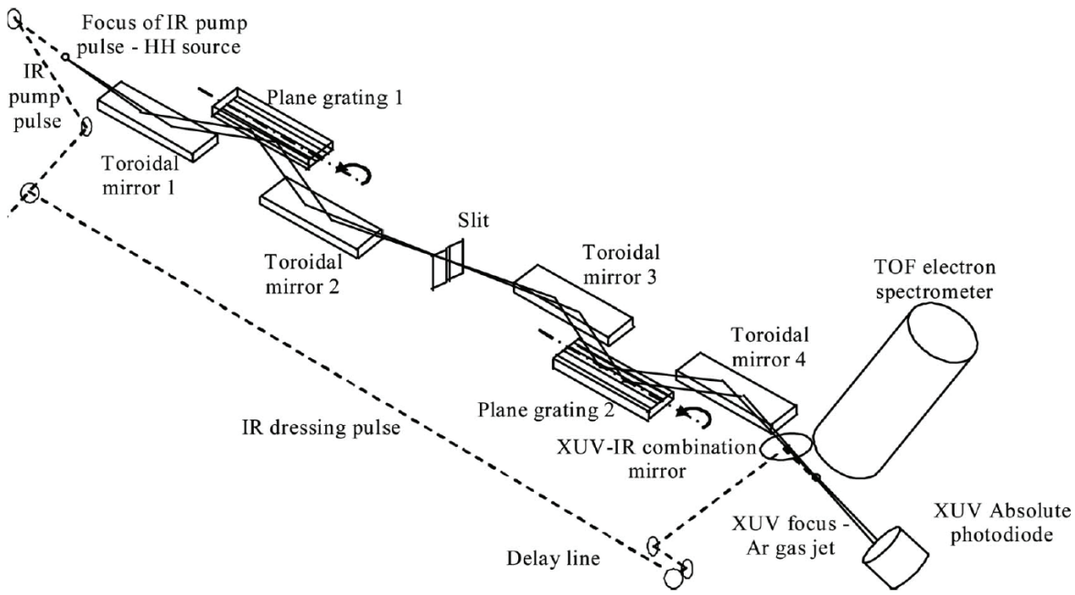

Fig. 14. Experimental setup to emasure the duration of the XUV pulse at the output of the TDC monochromator.

The XUV pulse ionizes Argon in the presence of the infrared field; when the two pulses overlap in time and space on the gas jet, sidebands appear in the photoelectron spectrum, spectrally shifted by the infrared photon energy, determined by the absorption of one harmonic photon plus either the absorption or the emission of one infrared photon. The sideband amplitude as a function of the delay τ between the XUV and infrared pulses provides the cross-correlation signal. Fig. 15 show (dots) the temporal evolution of the amplitude of the first sideband vs delay for H19 and H23. The measured cross-correlation traces can be well fitted assuming an XUV pulse duration T_X =13±0.5 fs FWHM for H19 and

T_X =8±1 fs FWHM for H23. The relative durations of the XUV and generating pulses turn out to be in good agreement with what expected from numerical simulations, which show that for plateau harmonics, as the case of H19, $T_X \approx T_0/2$, where T_0 is the duration of the generating pulse (25 fs in our case), while the XUV duration decreases in the cut-off region (Sansone et al., 2004). To our knowledge, this was the first measurement to confirm the ability of the double-grating configuration to make the spectral selection of ultrashort pulses and preserve their duration.

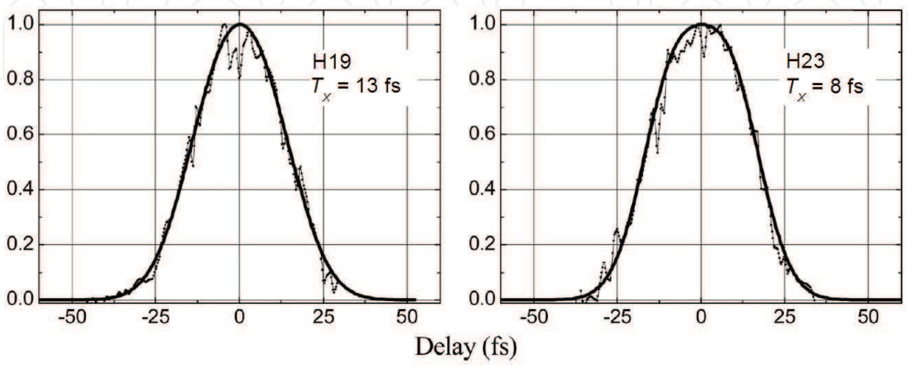

Fig. 15. Amplitude of the first sideband for H19 and H23 as a function of the delay between the XUV and IR pulses. The dots are the experimental results. T_X is the retrieved XUV pulse duration

The off-plane mount of the gratings is the core of the design of the TDC monochromator: it assures high efficiency, tunability in a broad spectral region, good focusing properties and compensation of the optical paths in the femtoseconds time scale.

6. Design of a double-grating attosecond compressor for ultrashort pulses

Radiation generated with the scheme of HHs by the use of laser pulses of few optical cycles is at present the tool for the investigation of matter with attosecond time resolution (Marciak-Kozlowska, 2009). The generation of trains of pulses (Paul et al., 2001; Lopez-Martens et al., 2005) as well as of isolated bursts (Kienberger et al., 2004; Sansone et al., 2006) of radiation in XUV region has been experimentally demonstrated. In both cases, the pulses are positively chirped as the result of the different duration of the quantum paths that contribute to the different portions of the emitted spectrum, so they can be compressed by introducing a suitable device with a negative group-delay-dispersion (GDD). This has been performer successfully by using a thin metallic aluminum filter. The main drawbacks of this compression method are the filter absorption, which may exceed one order of magnitude, and, even more, the rigidity of the compressor properties, as they derive from the elemental properties of the foil. For example, by using the polarization grating technique with neon as a target atom, the generation of pulses at 45 eV with a large spectrum that supports sub-100-as duration has occurred (Sola et al., 2006b), but not compressed so far for lack of suitable filter elements.

We present here a design of an instrument that aims to solve the problem of temporal compression of attosecond pulses by exploiting the influence on the pulse phase of a grating

compressor. Its design develops from the scheme of the double-grating TDC monochromator already discussed by a careful analysis of the effect on the phase of the ultrashort pulses.

The optical layout of the compressor is shown in Fig. 16. The design is similar to the TDC monochromator, but the toroidal mirrors are substituted by parabolic mirrors. The four mirrors are operated at equal grazing angle and at unity magnification, i.e., the input arm p of the collimators is equal to the output arm p of the focusers. The choice of parabolic mirrors is resulting from the analysis of residual aberrations in the optical path lengths, which shows that the use of the more simple toroidal mirrors is unacceptable for the brevity of the compressed pulses under study. After the reflection on P1, the beam is collimated and propagates toward G1. The azimuth α_1 of the incident rays on G1 is the same for all the wavelengths. The radiation is diffracted at the azimuth angle $\beta_1(\lambda)$ and collected by P2, which realizes a spectrally dispersed image of the source on its focal plane. This is the source plane for the second section of the compressor. Due to the symmetry of the configuration, the azimuth angle $\alpha_2(\lambda)$ of incident rays on G2 is equal to the azimuth angle $\beta_1(\lambda)$. Since the gratings are equal and operated at the same altitude, the azimuth angle β_2 of the rays diffracted from G2 is constant with the wavelength and equal to α_1. Finally, the rays are focused on the output focal point by P4. As in the case of the TDC monochromator, the design satisfies the condition of time-delay compensation, i.e., the differences in the path lengths of rays with the same wavelength but with different entrance directions within the beam aperture that are caused by the first grating are compensated by the second grating.

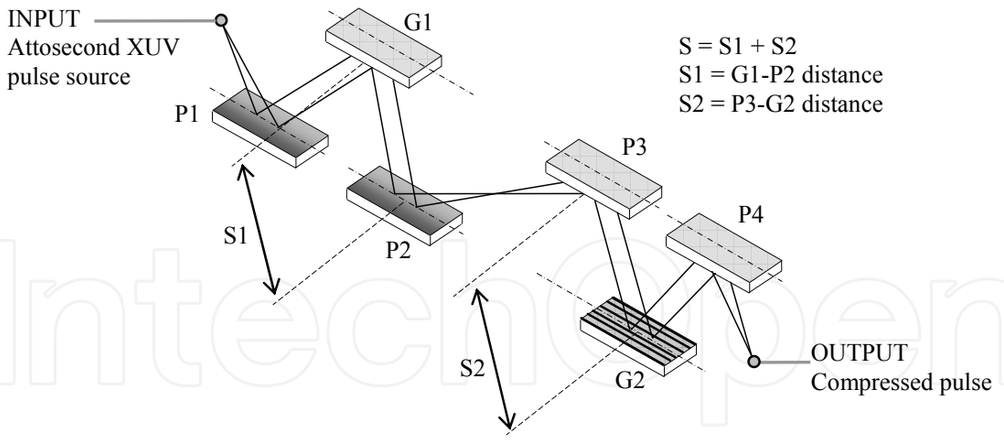

Fig. 16. Layout of the XUV attosecond compressor.

Since rays at different wavelengths are diffracted by G1 at different azimuth angles, they do not make the same optical path. The group delay, intended as the propagation time of rays from the source point to the output focal point, is dependent on the wavelength. The condition for zero GDD is to have G1 imaged on G2, which is realized when

$$S = S1 + S2 = 2p \tag{8}$$

where S1 and S2 are, respectively, the distances G1–P2 and P3–G2. For $S < 2p$, G1 is imaged behind G2 and the resulting GDD is positive. For $S > 2p$, G1 is imaged before G2 and the resulting GDD is negative. The three cases are illustrated in Fig. 17.

The chirp of the pulse can be varied by changing S = S1 + S2. It is simpler to keep S1 constant and to finely adjust S2 for changing the GDD. The variation of S2 is performed by mounting G2 on a linear translator and moving it along an axis coincident with the straight line that connects G2 to P3. Since the beam diffracted from G2 is collimated in a constant direction, the radiation reflected from P4 is focused always on the same output point. Therefore, the compressor has no moving parts except the translation of G2 for the fine tuning of the GDD.

The modeling of the compressor is done by ray-tracing simulations. The group delay is calculated for different values of the distance *S*. The GDD is then defined as the derivative of the group delay with respect to the frequency. The higher effects on the phase of the pulse can be analogously calculated by successive derivatives.

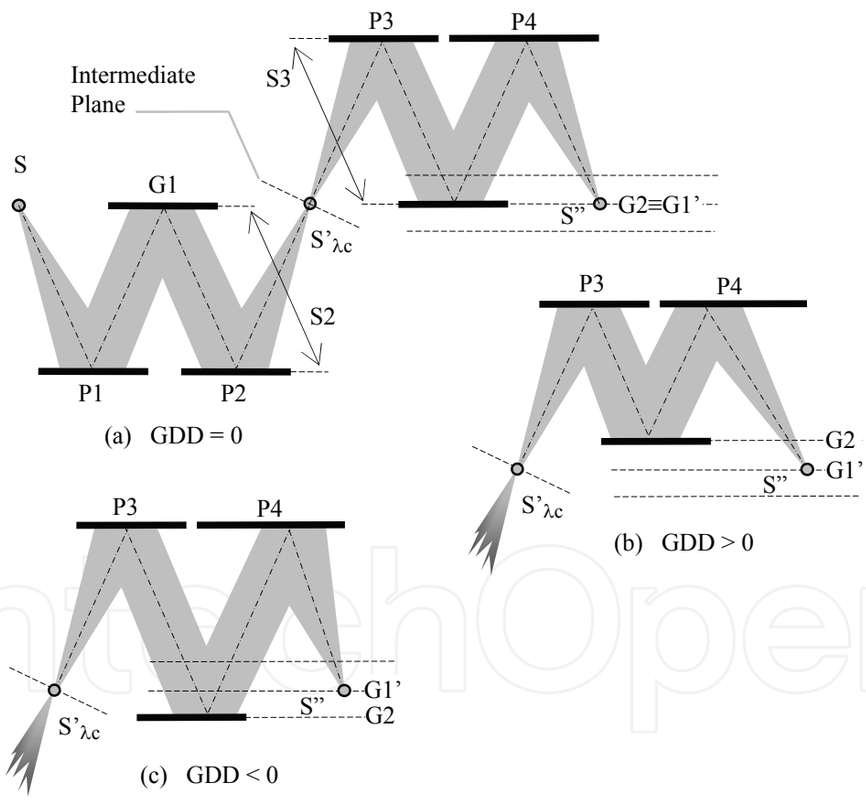

Fig. 17. Operation of the XUV attosecond compressor: a) GDD equal to zero; b) positive GDD; c) negative GDD.

As a test case of the optical configuration, the design of a compressor in the 12-24 nm region is presented. The grazing angle on the mirrors is chosen to be 3° for high reflectivity. The acceptance angle is 6 mrad, which matches the divergence of XUV ultrashort pulses. The size of the illuminated portion of the paraboloidal mirrors results 23 mm × 1.2 mm. On such

a small area, manufacturers routinely can produce paraboloidal mirrors with very-high quality finishing, both in terms of figuring errors (λ/30 at 500 nm) and of slope errors (less than 2 μrad rms). Since the gratings are ruled on plane substrates, the surface finishing is even better than on curved surfaces. Such precision on the optical surfaces is essential to have time-delay compensation in the range of tens of attoseconds. The altitude and blaze angles of the gratings have been selected to optimize the time-delay compensation.

Particular attention must be given to isolate the compressor optics from environmental vibrations and to precisely align the components in order to realize correct implementation of the optimal geometry.

The global efficiency of such a compressor can be predicted to be in the 0.10–0.20 range, on the basis of the efficiency measurements made on the existing off-plane monochromator and already discussed.

The time-delay compensation of the compressor has been analyzed with ray-tracing simulations. Once the grating groove density is selected, the time-delay compensation depends on the choice of altitude and azimuth angles. Both these parameters have to be optimized in order to minimize the residual spreads of the optical paths. In the case presented here, the choice of 200 gr/mm groove density, 1.5° altitude, and 4.3° azimuth gives a residual spread of less than 10 as FWHM in the whole 12-24 nm spectral region. The characteristics of the compressor are resumed in Tab. 5.

Pulse spectral interval	12-24 nm
Mirrors	**Off-axis paraboloidal**
Input/output arms	200 mm
Acceptance angle	6 mrad × 6 mrad
Grazing angle	3°
Size of illuminated area	23 mm × 1.2 mm
Gratings	**Plane**
Groove density	200 gr/mm
Altitude angle	1.5°
Blaze angle	4.5°
Distances	S > 400 mm for negative GDD

Table 5. Parameters of the compressor for the 12-24 nm region.

The calculated results of the compressor's phase properties are shown in Fig. 18. For $S > 400$ mm, the GDD is always negative as predicted and the values reported are in agreement with what is required to compress the pulse as resulting from the HH generation modeling.

An example of compression of a pulse with a positive GDD, modeled according to the results obtained using the polarization gating technique (Sola et al., 2006; Sansone et al., 2006), is presented in Fig. 19. Note the clear time compression to a nearly single-cycle pulse.

The scheme of the compressor is very versatile: it can be designed with high throughput in any spectral interval within the 4-60 nm XUV region. By a simple linear translation of a single grating, the instrument introduces a variable group delay in the range of few hundreds attoseconds with constant throughput and either negative or positive group-delay dispersion. The extended spectral range of operation and the versatility in the control of the

group delay allows the compression of XUV attosecond pulses beyond the limitations of the schemes based on metallic filters.

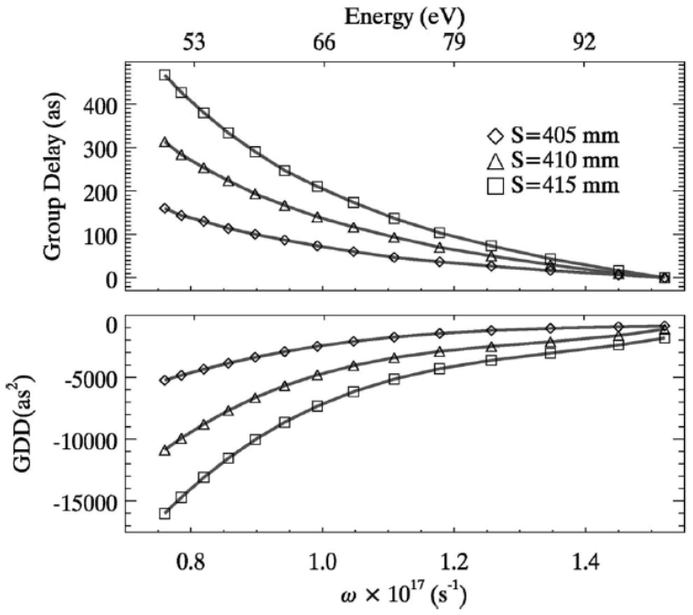

Fig. 18. Phase properties of the compressor with the parameters listed in Tab. 5: group delay (top) and group-delay dispersion (GDD).

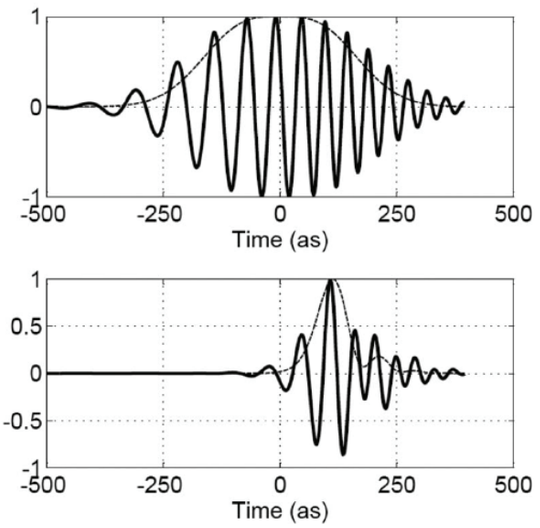

Fig. 19. Simulation of the compression of a chirped XUV pulse at the output of the compressor with the parameters listed in Tab. 5. Input pulse parameters: central energy 73 eV (17 nm), bandwidth 25 eV (6 nm), positive chirp with GDD = 5100 as^2. Compressor: S = 410 mm. FWHM durations: input 350 as, output 75 as.

7. Conclusions

The use of diffraction gratings to perform the spectral selection of ultrashort pulses in the XUV spectral region has been discussed. The main applications of such technique are the spectral selection of high-order laser harmonics and free-electron-laser pulses in the femtosecond time scale.

The realization of monochromators tunable in a broad spectral band in the XUV requires the use of gratings at grazing incidence. Obviously, the preservation of the time duration of the pulse at the output of the monochromator is crucial to have both high temporal resolution and high peak power. A single grating gives a temporal broadening of the ultrafast pulse because of the diffraction. This effect is negligible for picosecond or longer pulses, but is dramatic in the femtosecond time scale. Nevertheless, it is possible to design grating monochromators that do not alter the temporal duration of the pulse in the femtosecond time scale by using two gratings in a time-delay compensated configuration. In such a configuration, the second grating compensates for the time and spectral spread introduced by the first one.

Therefore, the grating monochromators for ultrafast pulses are divided in two main families:

1. the single-grating configuration, that gives intrinsically a temporal broadening of the ultrafast pulse, but is simple and has high efficiency since it requires the use of one grating only;
2. the time-delay compensated configuration with two gratings, that has a much shorter temporal response, in the femtosecond or even shorter time scale, but is more complex and has a lower efficiency.

Once the experimental requirements are given, aim of the optical design is to select the configuration that gives the best trade-off between time response and efficiency.

The efficiency is obviously the major factor discriminating among different designs: an instrument with low efficiency could be not useful for scientific experiments. An innovative configuration to realize monochromators with high efficiency and broad tunability has been discussed. It adopts gratings in the off-plane mount, in which the incident light direction belongs to a plane parallel to the direction of the grooves. The off-plane mount has efficiency higher than the classical mount and, once the grating groove density has been selected, it gives minimum temporal response at grazing incidence.

Both single- and double-grating monochromators in the off-plane mount can be designed. In particular, we have presented in details two applications to the selection of high-order harmonics, one using a single-grating design and one in a time-delay compensated configuration. In the latter case, the XUV temporal response at the output of the monochromator has been measured to be as short as few femtoseconds, confirming the temporal compensation given by the double-grating design.

Finally, the problem of temporal compression of broadband XUV attosecond pulses by means of a double-grating compressor has been addressed. The time-delay compensated design in the off-plane configuration has been modified to realize an XUV attosecond compressor that can introduce a variable group-delay dispersion to compensate for the intrinsic chirp of the attosecond pulse.

This class of instruments plays an important role for the photon handling and conditioning of future ultrashort sources.

8. Acknowledgment

The authors would like to remember the essential contribution of Mr. Paolo Zambolin (1965-2005) to the mechanical design of the time-delay compensated monochromator at LUXOR (Padova, Italy). The experiments on the beamline ARTEMIS at Rutherford Appleton Laboratory (UK) are carried on under the management of Dr. Emma Springate and Dr. Edmund Turcu. The experiments with high-order harmonics at Politecnico Milano (Italy) are carried on under the management of Prof. Mauro Nisoli and Dr. Giuseppe Sansone.

9. References

Akhmanov, S. A.; Vysloukh, V. A. & Chirkin, A. S. (1992) *Optics of Femtosecond Laser Pulses,* American IOP, New York

Cash, W. (1982). Echelle spectrographs at grazing incidence, *Appl. Opt.* Vol. 21, pp. 710–717

Corkum, P.B. & Krausz, F. (2007). Attosecond science. *Nat. Phys.* Vol. 3, pp. 381-387

Chiudi Diels, J.-C.; Rudolph, W. (2006). *Ultrashort Laser Pulse Phenomena,* Academic Press Inc., Oxford

Frassetto, F.; Bonora, S.; Villoresi, P.; Poletto, L.; Springate, E.; Froud, C.A.; Turcu, I.C.E.; Langley, A.J.; Wolff, D.S.; Collier, J.L.; Dhesi, S.S. & Cavalleri, A. (2008). Design and characterization of the XUV monochromator for ultrashort pulses at the ARTEMIS facility, *Proc. SPIE* Vol. 7077, Advances in X-Ray/EUV Optics and Components III, no. 707713, S. Diego (USA), August 2008, SPIE Publ., Bellingham

Frassetto, F.; Villoresi, P. & Poletto, L. (2008). Optical concept of a compressor for XUV pulses in the attosecond domain, *Opt. Exp.* Vol. 16, pp. 6652-6667

Kienberger, R. & Krausz, F. (2004). Subfemtosecond XUV Pulses: Attosecond Metrology and Spectroscopy, in *Few-cycle laser pulse generation and its applications*, F.X. Kärtner ed., pp. 143-179, Springer, Berlin

Kienberger, R.; Goulielmakis, E.; Uberacker, M.; Baltuska, A.; Yakovlev, V.; Bammer, F.; Scrinzi, A.; Westerwalbesloh, T.; Kleineberg, U.; Heinzmann, U.; Drescher, M. & Krausz, F. (2004). Atomic transient recorder, *Nature* Vol. 427, pp. 817-822

Jaegle', P. (2006). *Coherent Sources of XUV Radiation,* Springer, Berlin

Lopez-Martens, R.; Varju, K.; Johnsson, P.; Mauritsson, J.; Mairesse, Y.; Salières, P.; Gaarde, M.B.; Schafer, K.J.; Persson, A.; Svanberg, S.; Wahlström, C.-G. & L'Huillier, A. (2005). Amplitude and phase control of attosecond light pulses, *Phys. Rev. Lett.* Vol. 94, no. 033001

Marciak-Kozlowska, J. (2009). *From Femto-to Attoscience and Beyond,* Nova Science Publishers Inc., New York

Patel, N. (2002). Shorter, Brighter, Better. *Nature* Vol. 415, pp. 110-11

Petit, R. (1980). *Electromagnetic theory of gratings*, Springer, Berlin

Pascolini, M.; Bonora, S.; Giglia, A.; Mahne, N.; Nannarone, S. & Poletto, L. (2006) Gratings in the conical diffraction mounting for an EUV time-delay compensated monochromator, *Appl. Opt.* Vol. 45, pp. 3253-3562

Paul, P.M.; Toma, E.S.; Breger, P.; Mullot, G.; Auge, F.; Balcou, P.; Muller, H.G. & Agostini, P. (2001). Observation of a train of attosecond pulses from high harmonic generation, *Science* Vol. 292, pp. 1689–1692

Poletto, L. & Tondello, G. (2001). Time-compensated EUV and soft X-ray monochromator for ultrashort high-order harmonic pulses, *Pure Appl. Opt.* Vol. 3, pp. 374-379

Poletto, L.; Bonora, S.; Pascolini, M.; Borgatti, F.; Doyle, B.; Giglia, A.; Mahne, N.; Pedio, M. & Nannarone, S. (2004). Efficiency of gratings in the conical diffraction mounting for an EUV time-compensated monochromator, *Proc. SPIE* Vol. 5534, Fourth Generation X-Ray Sources and Optics II, pp. 144–153, Denver (USA), August 2004, SPIE Publ., Bellingham

Poletto, L. (2004). Time-compensated grazing-incidence monochromator for extreme-ultraviolet and soft X-ray high-order harmonics, *Appl. Phys. B* Vol. 78, pp. 1013-1016

Poletto, L. & Villoresi, P. (2006). Time-compensated monochromator in the off-plane mount for extreme-ultraviolet ultrashort pulses, *Appl. Opt.* Vol. 45, pp. 8577-8585

Poletto, L.; Villoresi, P.; Benedetti, E.; Ferrari, F.; Stagira, S.; Sansone, G.; Nisoli, M. (2007). Intense femtosecond extreme ultraviolet pulses by using a time-delay compensated monochromator, *Opt. Lett.* Vol. 32, pp. 2897-2899

Poletto, L.; Villoresi, P.; Benedetti, E.; Ferrari, F.; Stagira, S.; Sansone, G.; Nisoli, M. (2008). Temporal characterization of a time-compensated monochromator for high-efficiency selection of XUV pulses generated by high-order harmonics, *J. Opt. Soc. Am. B* Vol. 25, pp. B44-B49

Poletto, L.; Frassetto, F. & Villoresi, P. (2008). Design of an Extreme-Ultraviolet Attosecond Compressor, *J. Opt. Soc. Am. B* Vol. 25, pp. B133-B136

Poletto, L. (2009). Tolerances of time-delay compensated monochromators for extreme-ultraviolet ultrashort pulses, *Appl. Opt.* Vol. 48, pp. 4526-4535

Saldin, E.L.; Schneidmiller, E.A. & Yurkov, M.V. (2000). *The Physics of Free Electron Lasers*, Springer, Berlin

Sansone, G.; Vozzi, C.; Stagira, S. & Nisoli, M. (2004). Nonadiabatic quantum path analysis of high-order harmonic generation: role of the carrier-envelope phase on short and long paths, *Phys. Rev. A* Vol. 70, no. 013411

Sansone, G.; Benedetti, E.; Calegari, F.; Vozzi, C.; Avaldi, L.; Flammini, R.; Poletto, L.; Villoresi, P.; Altucci, C.; Velotta, R.; Stagira, S.; De Silvestri, S. & Nisoli, M. (2006). Isolated single-cycle attosecond pulses, *Science* Vol. 314, pp. 443–446

Sola, J.; Mevel, E.; Elouga, L.; Constant, E.; Strelkov, V.; Poletto, L.; Villoresi, P.; Benedetti, E.; Caumes, J.-P.; Stagira, S.; Vozzi, C.; Sansone, G. & Nisoli, M. (2006). Controlling attosecond electron dynamics by phase-stabilized polarization gating, *Nat. Phys.* Vol. 2, pp. 319–322

Villoresi, P. (1999). Compensation of optical path lengths in extreme-ultraviolet and soft-x-ray monochromators for ultrafast pulses, *Appl. Opt.* Vol. 38, pp. 6040-6049

Walmsley, I.; Waxer, L. & Dorrer, C. (2001). The role of dispersion in ultrafast optics, *Rev. Sci. Instr.* Vol. 72, pp. 1–28

Werner, W. (1977). X-ray efficiencies of blazed gratings in extreme off-plane mountings, *Appl. Opt.* Vol. 16, pp. 2078–2080

Werner, W. & Visser, H. (1981). X-ray monochromator designs based on extreme off-plane grating mountings, *Appl. Opt.* Vol. 20, pp. 487-492

Wiedemann, H. (2005). *Synchrotron Radiation,* Springer, Berlin

Wieland, M.; Frueke, R.; Wilhein, T.; Spielmann, C.; Pohl, M. & Kleinenberg, U. (2002) Submicron extreme ultraviolet imaging using high-harmonic radiation, *Appl. Phys. Lett.* Vol. 81, pp. 2520-2522

Advances in Solid State Lasers Development and Applications

Edited by Mikhail Grishin

ISBN 978-953-7619-80-0
Hard cover, 630 pages
Publisher InTech
Published online 01, February, 2010
Published in print edition February, 2010

Invention of the solid-state laser has initiated the beginning of the laser era. Performance of solid-state lasers improved amazingly during five decades. Nowadays, solid-state lasers remain one of the most rapidly developing branches of laser science and become an increasingly important tool for modern technology. This book represents a selection of chapters exhibiting various investigation directions in the field of solid-state lasers and the cutting edge of related applications. The materials are contributed by leading researchers and each chapter represents a comprehensive study reflecting advances in modern laser physics. Considered topics are intended to meet the needs of both specialists in laser system design and those who use laser techniques in fundamental science and applied research. This book is the result of efforts of experts from different countries. I would like to acknowledge the authors for their contribution to the book. I also wish to acknowledge Vedran Kordic for indispensable technical assistance in the book preparation and publishing.

How to reference

In order to correctly reference this scholarly work, feel free to copy and paste the following:

Luca Poletto, Paolo Villoresi and Fabio Frassetto (2010). Diffraction Gratings for the Selection of Ultrashort Pulses in the Extreme-Ultraviolet, Advances in Solid State Lasers Development and Applications, Mikhail Grishin (Ed.), ISBN: 978-953-7619-80-0, InTech, Available from: http://www.intechopen.com/books/advances-in-solid-state-lasers-development-and-applications/diffraction-gratings-for-the-selection-of-ultrashort-pulses-in-the-extreme-ultraviolet

INTECH
open science | open minds

InTech Europe
University Campus STeP Ri
Slavka Krautzeka 83/A
51000 Rijeka, Croatia
Phone: +385 (51) 770 447
Fax: +385 (51) 686 166
www.intechopen.com

InTech China
Unit 405, Office Block, Hotel Equatorial Shanghai
No.65, Yan An Road (West), Shanghai, 200040, China
中国上海市延安西路65号上海国际贵都大饭店办公楼405单元
Phone: +86-21-62489820
Fax: +86-21-62489821

IntechOpen